Multi-Scenario Radiative Human Body Cooling with a Selective Emission-Transmission Textile

Xueke Wu
Tsinghua University
Jinlei Li
Nanjing University
Qinyuan Jiang
Tsinghua University
Wenshuo Zhang
Tsinghua University
Baoshun Wang
Tsinghua University
Run Li
Tsinghua University
Siming Zhao
Tsinghua University
Fei Wang
Tsinghua University
Ya Huang
Tsinghua University
Pei Lyu
Tsinghua University
Yanlong Zhao
Tsinghua University
Jia Zhu
Nanjing University https://orcid.org/0000-0002-2871-4369
Rufan Zhang (zhangrufan@tsinghua.edu.cn)
Tsinghua University https://orcid.org/0000-0003-1774-0550

Article

Keywords:

Posted Date: August 30th, 2022

DOI: https://doi.org/10.21203/rs.3.rs-1991851/v1

Version of Record: A version of this preprint was published at Nature Sustainability on August 14th, 2023.
See the published version at https://doi.org/10.1038/s41893-023-01200-x.

Abstract

Radiative cooling (RC) is a promising sustainable human body cooling technology. However, there still lacks a RC material that can simultaneously enable efficient human body cooling in both outdoor and indoor hot scenarios. Here, we propose a selective emission-transmission (SET) RC model, which is featured with selective high emission in the atmospheric window waveband (8-13 μm) and high transmission in the remaining mid-infrared wavebands, to guide the design of multi-scenario RC materials. Assisted with designs at molecular and nano-scale, we demonstrated a polyoxymethylene (POM) nano-textile, which selectively exhibits high emittance of 75.7% in the 8-13 μm waveband, high human radiation transmittance of 48.5% (4-25 μm), and also a high solar reflectance of 94.7% (0.3-2.5 μm). As a result, the POM nano-textile exhibits superior human body cooling performance in various scenarios including sunny outdoor (2.6-8.8 ℃ cooling), cloudy outdoor (0.7-3.6 ℃ cooling) and indoor (0.5-1.2 ℃ cooling), compared to existing RC materials and commercial cotton. In addition, the POM nano-textile also possesses good wearability. When the POM nano-textile is tailored onto a protective clothing, it provides better cooling performance than its commercial counterpart. This work provides an alternative pathway towards multi-scenario personal thermal management.

full text

Nowadays, widely used active cooling systems such as air conditioners consume a lot of electrical energy (~ 15% of global electricity)[1,2]. Passive radiative cooling (RC), a zero energy-consuming technology for cooling by radiative heat transfer into surrounding environments with a lower temperature and even into the cold out space (nearly 3 K) through the atmospheric window (8–13 μm), has been proposed as a promising cooling technology[3–5]. RC technology has shown great potential for personal thermal management because the radiative heat transfer is actually the primary heat dissipation pathway for human bodies, which accounts for 40%~60% of the total heat transfer from a human body (Supplementary Fig. 1)[6,7].

Various RC materials have been developed for human body cooling in different indoor or outdoor scenarios[8–16]. According to their cooling mechanism, RC materials can be categorized into two types, transmission-type RC materials mainly used in indoor scenarios (Fig. 1a), and emission-type RC materials mainly used in outdoor scenarios (Fig. 1b). The transmission-type RC textile is transparent to human body radiation in the mid-infrared (MIR) waveband (Fig. 1d)[5,6,8]. Thus, human bodies (~ 34 ℃) can be cooled by directly dissipating heat through this textile into surrounding environments with low temperature, which has been proven to be the optimal choice for indoor radiative human body cooling[8,17]. In comparison, an emission-type RC textile emits the human heat into the cold outer space via the atmospheric window (8–13 μm) (Fig. 1e)[17–22]. Direct heat exchange with outer space and high solar reflection endow emission-type RC materials with the ability to achieve sub-ambient cooling effect under strong direct sunlight, making them an ideal choice for outdoor human body cooling[12,15,16,23–26].

It will be ideal for RC materials to enable effective human body cooling for both outdoor and indoor scenarios. However, for the transmission-type RC materials, they exhibit poor cooling performance when exposed to a hot outdoor scenario due to the massive solar thermal load (low solar reflectance) caused by thin thickness limitation[5,9,27,28]. Although several efforts have been made to improve the solar reflectance of such materials[10,17], balancing human body compatibility (such as harmlessness and comfortability) and high cooling performance remains a challenge. Also, for the emission-type RC materials to enable high cooling performance, there need to be a clear atmospheric window to send the radiative heat to the outer space. Therefore, when they are used in indoor scenarios, as the channel for radiative heat transfer into the outer space does not exist, the cooling performance is largely compromised[8]. In addition, even for the outdoor scenario, this atmospheric window is partially or completely blocked during cloudy days, leading to substantially decreased cooling performance[29–31]. Therefore, to design a multi-scenario RC material that possess high cooling performances in various scenarios, including cloudy outdoor, sunny outdoor, and indoor, it is critical but remain challenging to precisely tune the optical properties of a material in multiple wavelength bands (including the atmospheric window, non-window of MIR, and solar wavebands) to combine the advantages of both emission-type and transmission-type RC materials.

Selective emission-transmission model

Here, we propose a selective emission-transmission (SET) hybrid-type RC model to achieve multi-scenario human body cooling effect (Fig. 1c). The MIR spectral characteristic is shown in Fig. 1f. The SET hybrid-type RC (SET-type for short) textile exhibits emission-type characteristic in the atmospheric window (8–13 μm) and transmission-type characteristic outside the window, rendering it with an optimal emissive cooling effect by fully exploiting atmospheric window[20,28] while retaining transmissive cooling capacity for most human body radiation (~ 61%, inset of Fig. 1f). In addition, its semi-transparent characteristic benefiting from the carful molecular-scale design breaks the thickness limitation of transmission-type textiles and is expected to achieve high solar reflectance similar to emission-type textiles through nanostructured regulation. Thus, in outdoor scenarios, the SET-type textile can achieve human body cooling through both MIR emission and MIR transmission, while in indoor scenarios, its cooling performance is only slightly lower than that of transmission-type textiles but significantly better than that of emission-type textiles. Therefore, the SET-type textile is suitable for both outdoor and indoor scenarios, which is further demonstrated by the following theoretical calculations (Fig. 1g) and the mechanism is shown in Fig. 1c. Cooling performances of different types of textiles (emission-type, transmission-type, and SET-type) in outdoor and indoor scenarios were evaluated and compared numerically by solving steady state heat transfer models (Supplementary Figs. 2,3 and Supplementary Tables 1,2). The results showed that in outdoor scenarios under strong sunlight (800 W/m^2), the SET-type textile exhibited a significantly lower skin surface temperature than transmission-type (25.7°C lower) and emission-type (4.2°C lower) textiles (Figs. 1g,h). For indoor scenarios, the skin surface temperature with the SET-type textile was slightly higher (0.6°C) than that with transmission-type textiles but significantly lower (1.7°C)

than that with emission-type textiles (Fig. 1i). Therefore, the SET-type textile exhibited good performance in both outdoor and indoor scenarios.

Based on the above results, we developed a polyoxymethylene (POM) nano-textile with the SET characteristics (denoted as SET-type POM textile) for the desired multi-scenario human body cooling. The synthesized SET-type POM textile exhibited 75.7% selective emittance at the 8–13 μm waveband (a high selectivity of 1.67, which is the ratio of average emittance between the 8–13 μm and 4–25 μm ranges), 48.5% transmittance at the 4–25 μm waveband, and 94.6% solar reflectance at the 0.3–2.5 μm waveband, making it an ideal SET-type RC material. As a result, the SET-type POM textile exhibited a significantly enhanced radiative human body cooling performance that was better than those of typical transmission-type, emission-type, and commercial cotton textiles in sunny outdoor (7.8, 2.6, and 8.8°C cooler, respectively), cloudy outdoor (2.9, 0.7, and 3.6°C cooler, respectively), and indoor scenarios (-0.2, 1.2, and 0.5°C cooler, respectively). Furthermore, the SET-type POM textile also exhibited good breathability, high tensile strength, and good anti-humidity capability. The field test demonstrated that a SET-type POM textile-based health hazard protective clothing showed significantly better cooling performance than a commercial counterpart in sunny outdoor (5.4 ℃ cooler), cloudy outdoor (1.3 ℃ cooler), and indoor scenarios (~ 1.0 ℃ cooler).

Material design and characterization

Emission and transmission by organic materials in the MIR region depend on their molecular bonds/functional groups, which have vibrational absorption/emission in different waveband ranges[32,33]. For the ideal high performance SET-type textiles, the vibrational absorption/emission frequencies of their molecular bonds/functional groups should be restricted to the atmospheric window waveband (8–13 μm). Common functional groups of polymers and their wavelength ranges in the MIR region (4–25 μm) are listed in Fig. 2a. Based on the careful screening and analysis of these functional groups, POM, a widely used polymer with a backbone chain consisting only of C-O-C bonds, was expected to have SET characteristics. This was experimentally confirmed by attenuated total reflection (ATR) mode Fourier transform infrared spectroscopy (FTIR, Fig. 2b)[34,35]. The characteristic peaks of the FTIR-ATR curve show that the wavelengths of the vibrational absorption/emission of POM are mainly distributed in the atmospheric window (8–13 μm) (Supplementary Table 3), indicating that POM is a promising SET-type textile.

In addition to the selective MIR emission and transmission, a strong solar reflectance is also necessary for RC materials for daytime outdoor scenarios. However, commercial POM products exhibit a low solar reflectance (~ 49.0%, Supplementary Fig. 4). According to the Mie scattering theory[8,28], a fiber-based textile would exhibit high solar scattering efficiency when its fiber diameter distribution is close to the waveband of the solar spectrum (Fig. 2a). Therefore, POM nanofibers with a diameter distribution close to the solar waveband are expected to exhibit strong solar reflectance for daytime outdoor scenarios.

Based on the above analysis, a hierarchical SET-type POM nanofiber textile with a thickness of ~ 260 μm was synthesized through electrospinning (Fig. 2c, Supplementary Figs. 5,6). The synthesized POM nanofibers were randomly stacked on each other and exhibited a rough surface (Fig. 2d and Supplementary Fig. 7). The diameter size distribution of these POM nanofibers is close to the main solar waveband of 0.3-1.0 μm (Fig. 2e). In addition to the suitable nanofiber diameters, the disordered arrangement and rough surface of the POM nanofibers also contribute a lot to the high solar reflectance of the POM textile (Supplementary Fig. 8)[28]. Characterization showed that the synthesized POM textile exhibits a high solar reflectance of 94.6% in the waveband of 0.3–2.5 μm (Fig. 2f), and in the main solar waveband of 0.3–1.5 μm, the average reflectance reached 95.2%. In comparison, in the MIR region of 4–25 μm, the POM textile exhibited an ultra-low reflectance of 6.3% (inset of Fig. 2f), meaning that it has a high MIR emittance/transmission and thus is an ideal non-reflective textile and a prerequisite component for SET-type textiles. More importantly, the SET-type POM textile selectively exhibits a high emittance of 75.9% in the atmospheric window of 8–13 μm (the selectivity reached 1.67) and an average transmittance of 70.0% outside the atmospheric window. Moreover, the average transmittance of the POM textile reaches 48.5% in the entire MIR region of 4–25 μm, indicating that it can transmit nearly half of a human body radiation. These results demonstrate that the synthesized SET-type POM textile exhibits the desired characteristics of the above SET hybrid-type RC model, and can be expected to provide multi-scenario human body cooling.

Thermal measurements

The multi-scenario radiative human body cooling performance of the synthesized SET-type POM textile was investigated with specially designed measurement devices (Figs. 3a,b) in three typical scenarios during hot summer in Nanjing, China (118°57'10" E, 32°07'14" N), which were sunny outdoor, cloudy outdoor, and indoor scenarios. Bare skin (uncovered skin simulator) and the skin with the three typical textiles (commercial cotton, emission-type polyvinylidene difluoride (PVDF), and transmission-type nanoporous polyethylene (PE)) were employed for comparison (Supplementary Figs. 9–11). As shown in Figs. 3c, the PVDF and PE textiles were chosen for their high emittance (90.0%) and transmittance (96.9%), respectively, in the entire MIR region, while the former also exhibits a high solar reflectance (95.0%) close to that of the SET-type POM textile. These samples were placed in similar measurement devices with each device consisting of a textile sample, a skin simulator, surrounding insulating foam, and a K type thermocouple for monitoring the real-time temperature of the skin simulator (as shown in Figs. 3a,b). Constant input power (140 W/m^2) was applied to the heaters to simulate the metabolic heat production rate of human skin. The skin simulators and thermocouples were carefully calibrated to ensure that the difference between measured temperatures was only caused by the difference between the different samples.

Figures 3d-g clearly show that in the outdoor scenarios (for both sunny and cloudy days, Supplementary Fig. 12), the SET-type POM textile covered skin simulator had the lowest surface temperature of the five samples. In the sunny scenario under strong direct sunlight (> 800 W/m^2, with peak solar irradiance of ~

935 W/m^2 and a high T_{amb} of 34.1 °C) from 10 a.m. to 1 p.m., the temperature of the SET-type POM textile covered skin simulator was lower than that of the bare skin and the skin covered by cotton, transmission-type PE, and emission-type PVDF by 15.7, 8.8, 7.8, and 2.6 °C, respectively (Figs. 3d,e and Supplementary Fig. 13). In a hot cloudy outdoor scenario (T_{amb} = 37.4 °C), the surface temperature of the SET-type POM textile covered skin simulator was also still much lower than the others by 5.5, 3.6, 2.9, and 0.7°C, respectively (Figs. 3f,g and Supplementary Fig. 14). The results indicate that the SET-type POM textile exhibits the best outdoor cooling performance for a human body. This was due to its higher average solar reflectance than that of bare skin, cotton (~ 68%, Supplementary Fig. 15), and transmission-type PE (~ 48.4%, Supplementary Fig. 11d), as well as its extra transmission effect when compared with emission-type PVDF.

The SET-type POM textile also exhibited good cooling performance in the indoor scenarios, which means allowing a higher air temperature setpoint of active cooling devices while maintaining human thermal comfort, which can save energy by ~ 7% per 1°C increase[8,36,37]. As shown in Figs. 3h,i, in a room at 30.4 °C, the temperature of the SET-type POM textile covered skin simulator was lower than that covered with emission-type PVDF and commercial cotton by 1.2 and 0.5 °C, respectively, while it was only 0.2 °C higher than that covered with transmission-type PE (Supplementary Fig. 16). That is, the human body cooling performance of the SET-type POM textile in an indoor scenario is close to that of the transmission-type PE and better than that of both the emission-type PVDF and commercial cotton textiles. A comprehensive consideration of the results in both indoor and outdoor thermal measurements, it is clear that the SET-type POM textile has the most effective cooling effect for the human body.

Wearability testing

In addition to the superior RC performance, the synthesized SET-type POM textile also exhibits many metrics required for wearability, namely, good breathability, mechanical strength, waterproofness, and anti-humidity capability. First, we measured the breathability of the SET-type POM textile, which refers to the ability of a textile to carry human body heat away across the textile by airflow under a pressure difference and is important for human comfort. As shown in Supplementary Fig. 17, when sandwiching the SET-type POM textile between water and air, continuous bubble penetration (Supplementary Movies 1 and 2) without any textile breakage clearly indicates its good breathability. As shown in Fig. 4a, quantitative air permeability tests further showed that the SET-type POM textile exhibits a similarly good breathability as a commercial cotton, which is due to its fluffy fibrous structure and specially designed pores (punched by a commonly used microneedling technique[8], Supplementary Fig. 18). In addition, the water vapor transmission rate was also measured, which represents the ability of a textile to transfer water vapor produced from perspiration evaporation. As shown in Fig. 4b and Supplementary Fig. 19, in the performance attributable to the existence of countless nano/micropore channels for water vapor permeation (Supplementary Figs. 6,20), the SET-type POM textile exhibits a high water vapor transmission rate (0.011 g/cm^2 hour), which is similar with commercial cotton and the above two types of RC textiles (0.010–0.012 g/cm^2 hour).

In addition, the SET-type POM textile also showed a high tensile strength of 13.3 MPa, which is comparable with that of the commercial cotton (14.7 MPa) (Figs. 4c). The high mechanical strength is attributed to the high crystallinity of the POM nanofibers (Supplementary Fig. 21) that have a high inherent strength (70 MPa)[38]. The elongation of the SET-type POM textile is the highest (~ 300%) among these different textiles (Fig. 4c and Supplementary Fig. 22), indicating its high flexibility for comfortable skin touch. The anti-humidity capability, which is important for keeping a textile dry and clean in humid environments, of these samples was also compared. The water contact angle of the SET-type POM textile reached 138° and still remained at 122°after half an hour, which were much higher than that of the other three textiles (Fig. 4d and Supplementary Fig. 23), indicating that the SET-type POM textile exhibits the highest waterproofness and anti-humidity capability.

We also tested the real performance of the SET-type POM textile on a protective clothing by sewing a POM cloth onto one side of the chest of the commercial protective clothing and the other side was retained for comparison (Figs. 4e,f, and Supplementary Fig. 24). The thermal properties of a researcher wearing the modified protective clothing were recorded in three typical scenarios (sunny outdoor, cloudy outdoor, and indoor scenarios). The clothing surface temperature was captured and visually presented using an infrared camera (Testo, 8–14 μm). As shown in Fig. 4g, in the outdoor scenarios (both sunny and cloudy), the clothing temperature on the SET-type POM textile section was lower than that on the counterpart section in the continuous test. In the sunny outdoor scenario under strong direct sunlight (> 800 W/m^2), the surface temperature difference between the two sides of the clothing reached nearly 3.0°C (Supplementary Movie 3). In the cloudy outdoor scenario with a solar irradiation of ~ 200 W/m^2, the temperature difference on the two-side cloth surface also reached nearly 1.5 ℃ (Fig. 4g and Supplementary Movie 4). Besides, the corresponding skin temperatures under the clothing were monitored in real-time by bead-probe thermocouples (Figs. 4h-k). In a similar sunny outdoor environment (Figs. 4h,i), the skin temperature difference tested by thermocouples reached 5.4°C, and the maximum difference even exceeded 6.0°C (Fig. 4i). Clearly, the SET-type POM textile shows huge potential in improving human thermal comfort under strong sunlight. The skin temperature difference was 1.3 ℃ in a similar cloudy outdoor environment (Figs. 4h,j). These results together demonstrate a significantly enhanced RC performance of the SET-type POM textile over that of commercial protective clothing in various outdoor scenarios.

Moreover, in the indoor environment, although the surface temperature of the clothing on both sides were similar with each other (Fig. 4g and Supplementary Movie 5), the skin temperature on the POM side was nearly 1.0°C lower than that on the commercial side (Figs. 4h,k). Thus, the SET-type POM textile also exhibited better indoor RC performance. Therefore, the SET-type POM textile exhibited superior cooling performance over that of commercial protective clothing in both outdoor and indoor scenarios and therefore has high commercialization potential.

Discussion

We proposed a SET hybrid type RC model for multi-scenario radiative human body cooling, and fabricated an SET-type POM textile based on the above model, which selectively exhibited an emittance of 75.7% in the atmospheric window (8–13 μm), a high human radiation transmittance of 48.5% (4–25 μm), and a high solar reflectance of 94.6% (0.3–2.5 μm). Due to the excellent SET property, the SET-type POM textile exhibited superior human body cooling performance over that of existing RC textiles and a commercial cotton textile in both outdoor and indoor scenarios (0.5–8.8°C cooler). The SET-type POM textile also exhibits good wearability, such as high breathability, good tensile strength, and anti-humidity capability. A SET-type POM textile-based protective clothing demonstrated superior practical cooling effect over that of a commercial one in both outdoor and indoor scenarios (1.0-5.4°C cooler). This work provides a novel solution to solve the incompatible needs of outdoor and indoor human body cooling, and provides a promising candidate for the next generation personal thermal management.

Methods

Fabrication of POM and PVDF textiles. 5 wt% POM solution was prepared by adding POM powder (commercial grade, Aladdin) into 1,1,1,3,3,3-hexafluoro-2-propanol (HFIP, 99%, Aladdin) while stirring. The mixture was then continuously stirred at 40°C for 2 h. The resulting homogeneous solution was electrospun using a 20-gauge needle tip with a voltage of 18 kV and a feed rate of 2 ml/h. The spinning distance, relative humidity, and temperature during spinning were kept at 18 cm, 40%, and 25°C, respectively. The PVDF textile was obtained using the same method. 13 wt% PVDF (Mv ~ 370000, Kynar) solution in a dimethylformamide (DMF, 99%, Aladdin) and acetone (AR, Tongguang) mixed solvent (4:1, v/v) was prepared. The mixture was continuously stirred at 50°C for 5 h. The resulting solution was electrospun using a 19-gauge needle tip with a voltage of 12 kV, a feed rate of 0.5 ml/h, and a spinning distance of 20 cm. The relative humidity and temperature were kept at ~ 40% and 32°C, respectively. Besides, nanoporous PE (~ 16 μm, AsahiKASEI, Japan) and commercial cotton (~ 300 μm) were obtained commercially.

Spectral characterization. The spectral properties of the POM textile were characterized separately in the solar spectrum (0.3–2.5 μm) and MIR (2.5–25 μm) wavebands. In the first range, the solar reflectance and transmission spectra were recorded using an ultraviolet-visible-near-infrared spectrophotometer (Cary 7000, Agilent) equipped with an integrating sphere model (Internal DRA-2500, Agilent). For the second range, a Fourier transform infrared spectrometer (FTIR, INVENIO, Bruker) equipped with a gold integrating sphere (A562, Bruker) was used to measure the absorption/emission and transmission spectra.

Morphology characterization. Optical images of the samples were taken by a digital camera (Nikon DSLR D5100). The microstructure of the POM textile was characterized by a scanning electron microscopy (JSM7900F).

Thermal measurements. The cooling effects of the different textiles were measured using the devices shown in Fig. 3a (schematic) and Fig. 3b (photograph). Human skin was simulated by a layered structure of Kapton heater/thermally conductive silicone grease/Cu plate/paint. The Kapton heater was connected

to a DC power source that provided ~ 140 W m^{-2} of heating power, which is the heat flux from a body's metabolic heat generation. The thermally conductive silicone grease and Cu plate with a thickness of 5 mm served as thermal connection and heat spreader, respectively, for a uniform temperature distribution. The paint was blended to have a skin-like spectrum in both the solar waveband and mid-infrared wavebands. Aluminum foil and foam in the test devices were utilized to minimize the thermal impact from the surrounding, which is a method used in previous works. K type thermocouples connected to a recorder (MIK-R6000C, Asmik) were used to monitor the samples' temperature in real time. The thermocouples were carefully calibrated with a test error of 0.4°C for the outdoor tests and 0.1°C for the indoor measurements. The ambient conditions (including input sunlight power, ambient temperature, and relative humidity) during the outdoor tests were measured and recorded by a weather station (TS-G1, Tuolaisi) adjacent to the test devices.

Wearability testing. Water vapor transmission rate test. The water vapor transmission rates of the POM textile, emission-type PVDF, transmission-type PE, commercial cotton, and normal PE sealing film were measured by the methods previously reported. Bottles (50 ml) filled with distilled water were sealed with the textile sample and rubber bands. These sealed bottles were kept in an environment with constant temperature (30°C) and relative humidity (40%). The weight of the sealed bottles was recorded every six hours for 72 hours. The WVTRs were obtained by dividing the reduction in mass due to water evaporation by the exposed area of the textile.

Air permeability test. (1) Qualitative testing. The POM textile was sealed between two pipes that were open above and sealed below. The exposed area of the textile was ~ 20 cm^2. The bottom pipe was connected to a compressed air source and the top pipe was filled with water and open to air. The gas permeability of the sample was qualitatively assessed by observing the air bubbles and membrane integrity after a constant flow rate of gas (20 sccm) was introduced. (2) The quantitative testing procedure was based on GB/T 24218.15–2018 (Chinese standard). The textile sample was sealed between two pipes. The exposed area of textile was 20 cm^2. One pipe was connected to a compressed air source and the other one was exposed to open air. A differential pressure gauge was connected to the two pipes to measure the pressure drop across the textile sample at different air flow rates. The air permeability of electrospun films decreases significantly with increasing thickness, which made our POM textile slightly less breathable than commercial cotton (Supplementary Fig. 20a). To represent the breathability of the POM textile in commercial applications, the above POM textile was punched with ~ 100 μm holes every 1 mm (invisible to the naked eye, Supplementary Figs. 20b,c) using the microneedling technique commonly used in the textile industry.

Mechanical test. The tensile strength tests of the POM textile, emissive-type PVDF, transmissive-type PE, and commercial cotton were measured by a Servo tensile testing machine (HZ-1004A). The samples had the same size (2 cm wide, 10-cm-long), and a gauge distance 6 cm long. The displacement rate was 10 mm/min.

Anti-humidity test (Contact angle versus time). The water contact angle of the textile sample was measured using a contact angle analyzer (XG-CAMA1) at a room temperature of ~ 25°C and an ambient relative humidity of ~ 40%. The contact angle for each sample was recorded continuously for half an hour.

Protective clothing testing. A commercial medical protective clothing (50% polypropylene non-woven fabric + 50% PE) was employed as a basis and reference. The modified protective clothing was obtained by sewing a POM cloth (~ 20×20 cm^2) onto one side of the chest of the commercial protective clothing (the commercial cloth at the corresponding position has been previously cut and removed, Supplementary Fig. 22). The commercial cloth on the other side was retained for comparison. The real-time surface temperatures of the clothing and human body were monitored using an infrared camera (Testo 890, 8–14 μm) and K type thermocouples, respectively. The corresponding solar irradiation was recorded with a solar power meter (TES-1333, TES). The tests were measured in sunny outdoor, cloudy outdoor, and indoor scenarios in Beijing, China (May 2022, 40°0'33" N, 116°20'0.6" E).

Declarations

Data availability

The data that support the findings of this paper are available from the corresponding authors upon reasonable request.

Received: xx; Accepted: xx; Published online: xx

Acknowledgments

This work is supported by the National Key Research and Development Program of China (2020YFA0210702, 2020YFC2201103) and the National Natural Science Foundation of China (22075163, 51872156).

Author contributions

R.Z., X.W., J.Z., and J.L. conceived the idea. X.W. and J.L. designed the models and experiments. X.W. and J.L. performed the material preparation and characterization with the help of J.Q., W.Z., B.W., R.L., S.Z., F.W., Y.H., Y.Z., and P. L. X.W. and J.Q. performed the modelling work. X.W. wrote the manuscript. R.Z. supervised the project. All the authors provided discussion and comments.

Competing interests

The authors declare no competing interests.

Additional information

Supplementary information The online version contains supplementary material available at https://doi.org/xxxx.

Correspondence and requests for materials should be addressed to J.Z. or R.Z.

Peer review information Nature Nanotechnology thanks xxx and the other, anonymous, reviewer(s) for their contribution to the peer review of this work.

Reprints and permissions information is available at www.nature.com/xxx.

References

1. Mitchard, E. T. A. The tropical forest carbon cycle and climate change. Nature **559**, 527–534, (2018).
2. *Heating and Cooling US Department of Energy*, <https://www.energy.gov/energysaver/heating-and-cooling>.
3. Yin, X., Yang, R., Tan, G. & Fan, S. Terrestrial radiative cooling: Using the cold universe as a renewable and sustainable energy source. Science **370**, 786–791, (2020).
4. Munday, J. N. Tackling Climate Change through Radiative Cooling. Joule **3**, 2057–2060, (2019).
5. Fan, S. & Li, W. Photonics and thermodynamics concepts in radiative cooling. Nat. Photonics **16**, 182–190, (2022).
6. Peng, Y. & Cui, Y. Advanced Textiles for Personal Thermal Management and Energy. Joule **4**, 724–742, (2020).
7. Fang, Y., Chen, G., Bick, M. & Chen, J. Smart textiles for personalized thermoregulation. Chem. Soc. Rev. **50**, 9357–9374, (2021).
8. Hsu, P. C. *et al.* Radiative human body cooling by nanoporous polyethylene textile. Science **353**, 1019–1023, (2016).
9. Zeng, S. *et al.* Hierarchical-morphology metafabric for scalable passive daytime radiative cooling. Science **373**, 692–696, (2021).
10. Cai, L. *et al.* Spectrally Selective Nanocomposite Textile for Outdoor Personal Cooling. Adv. Mater. **30**, 1802152, (2018).
11. Peng, Y. *et al.* Nanoporous polyethylene microfibres for large-scale radiative cooling fabric. Nat. Sustain. **1**, 105–112, (2018).
12. Leroy, A. *et al.* High-performance subambient radiative cooling enabled by optically selective and thermally insulating polyethylene aerogel. Sci Adv **5**, eaat9480, (2019).
13. Hsu, P. C. & Li, X. Q. Photon-engineered radiative cooling textiles. Science **370**, 784–785, (2020).
14. Kim, G., Park, K., Hwang, K. J. & Jin, S. Highly Sunlight Reflective and Infrared Semi-Transparent Nanomesh Textiles. ACS nano **15**, 15962–15971, (2021).
15. Zhu, B. *et al.* Subambient daytime radiative cooling textile based on nanoprocessed silk. Nat. Nanotechnol. **16**, 1342–1348, (2021).

16. Zhang, X. *et al.* A Moisture-Wicking Passive Radiative Cooling Hierarchical Metafabric. ACS nano **16**, 2188–2197, (2022).
17. Iqbal, M. I. *et al.* Radiative Cooling Nanofabric for Personal Thermal Management. ACS Appl. Mater. Interfaces **14**, 23577–23587, (2022).
18. Shi, N. N. *et al.* Keeping cool: Enhanced optical reflection and radiative heat dissipation in Saharan silver ants. Science **349**, 298–301, (2015).
19. Chen, Z., Zhu, L., Li, W. & Fan, S. Simultaneously and Synergistically Harvest Energy from the Sun and Outer Space. Joule **3**, 101–110, (2019).
20. Chen, Z., Zhu, L., Raman, A. & Fan, S. Radiative cooling to deep sub-freezing temperatures through a 24-h day-night cycle. Nat. Commun. **7**, 13729, (2016).
21. Bhatia, B. *et al.* Passive directional sub-ambient daytime radiative cooling. Nat. Commun. **9**, 5001, (2018).
22. Raman, A. P., Anoma, M. A., Zhu, L., Rephaeli, E. & Fan, S. Passive radiative cooling below ambient air temperature under direct sunlight. Nature **515**, 540–544, (2014).
23. Chen, Y. *et al.* Cellulose-Based Hybrid Structural Material for Radiative Cooling. Nano Lett. **21**, 397–404, (2021).
24. Mandal, J. *et al.* Hierarchically porous polymer coatings for highly efficient passive daytime radiative cooling. Science **362**, 315–318, (2018).
25. Li, T. *et al.* A radiative cooling structural material. Science **364**, 760–763, (2019).
26. Zhai, Y. *et al.* Scalable-manufactured randomized glass-polymer hybrid metamaterial for daytime radiative cooling. Science **355**, (2017).
27. Chen, M., Pang, D., Chen, X., Yan, H. & Yang, Y. Passive daytime radiative cooling: Fundamentals, material designs, and applications. EcoMat **4**, e12153, (2021).
28. Li, D. *et al.* Scalable and hierarchically designed polymer film as a selective thermal emitter for high-performance all-day radiative cooling. Nat. Nanotechnol. **16**, 153–158, (2021).
29. Han, D., Ng, B. F. & Wan, M. P. Preliminary study of passive radiative cooling under Singapore's tropical climate. Sol. Energy Mater. Sol. Cell **206**, (2020).
30. Godbole, R. V. Destabilization of Clouds by Radiative Cooling. Mon. Weather Rev. **101**, 496–500, (1973).
31. Huang, J. Y., Lin, C. J., Li, Y. & Huang, B. L. Effects of humidity, aerosol, and cloud on subambient radiative cooling. Int. J. Heat Mass Tran. **186**, (2022).
32. Zhou, Z., Wang, X., Ma, Y., Hu, B. & Zhou, J. Transparent Polymer Coatings for Energy-Efficient Daytime Window Cooling. Cell Rep. Phys. Sci. **1**, 100231, (2020).
33. Aili, A. *et al.* Selection of polymers with functional groups for daytime radiative cooling. Mater. Today Phys. **10**, 100127, (2019).
34. Di Noto, V., Angelini, E., Beltramini, M., Dalla Via, L. & Salvato, B. Fourier transform infrared attenuated total reflectance spectrometry of hemolymph and hemocyanin in water solutions. Vib. Spectrosc. **18**,

1–15, (1998).

35. Kennedy, E. R. & Ashley, K. Fourier-Transform Infrared Spectrometry Attenuated Total Reflectance Study of the Reaction of Pentanal and Propanal with 2-(Hydroxymethyl)Piperidine. Appl. Spectrosc. **46**, 266–272, (1992).
36. Hoyt, T., Arens, E. & Zhang, H. Extending air temperature setpoints: Simulated energy savings and design considerations for new and retrofit buildings. Build. and Environ. **88**, 89–96, (2015).
37. T. Hoyt, H. L. Kwang, H. Zhang & T. E. Arens. in *International Conference on Environmental Ergonomics* (Boston, 2009).
38. Kongkhlang, T. *et al.* Electrospun polyoxymethylene: Spinning conditions and its consequent nanoporous nanofiber. Macromolecules **41**, 4746–4752, (2008).

Figures

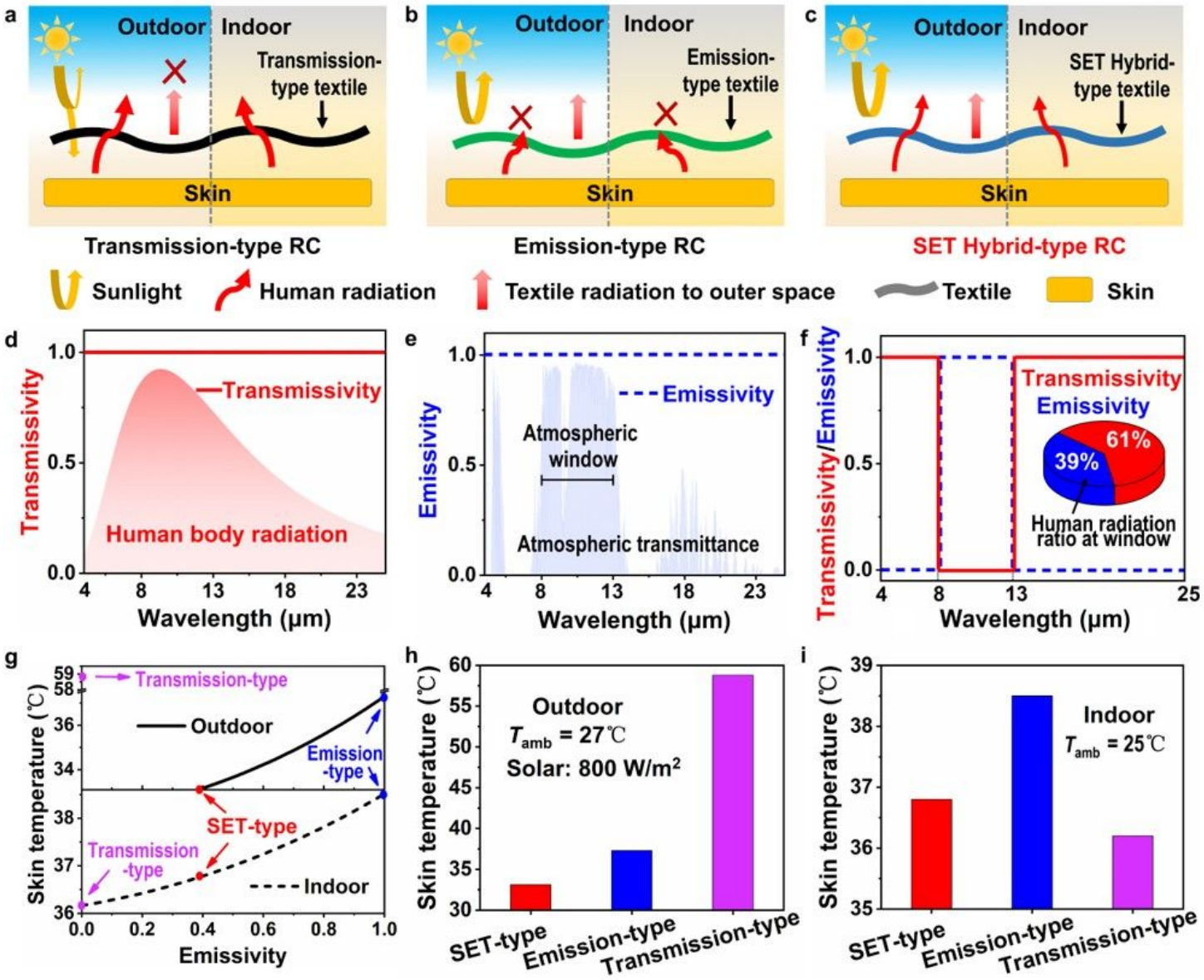

Figure 1

Design and model calculations of a selective emission-transmission (SET) hybrid RC textile. a-c, Schematic for radiative human body cooling models with transmission-type (**a**), emission-type (**b**), and SET hybrid-type (**c**) textiles. **d-f**, Corresponding spectral features in the mid-infrared region for the three different types of textile models. The first two models are completely transparent (**d**) and completely absorbed/emitted (**e**) with respect to human radiation, respectively. In comparison, the SET hybrid-type model (**f**) exhibits selective absorption/emission (39%) and partially transparent (61%) to human radiation. **g**, Simulated skin surface temperature calculated based on a function of MIR emittance of the textile at constant ambient temperature and human metabolic generation rate. **h**,**i**, Comparison of skin surface temperature corresponding to the three RC models in sunny outdoor (**h**) and indoor (**i**) scenarios, respectively.

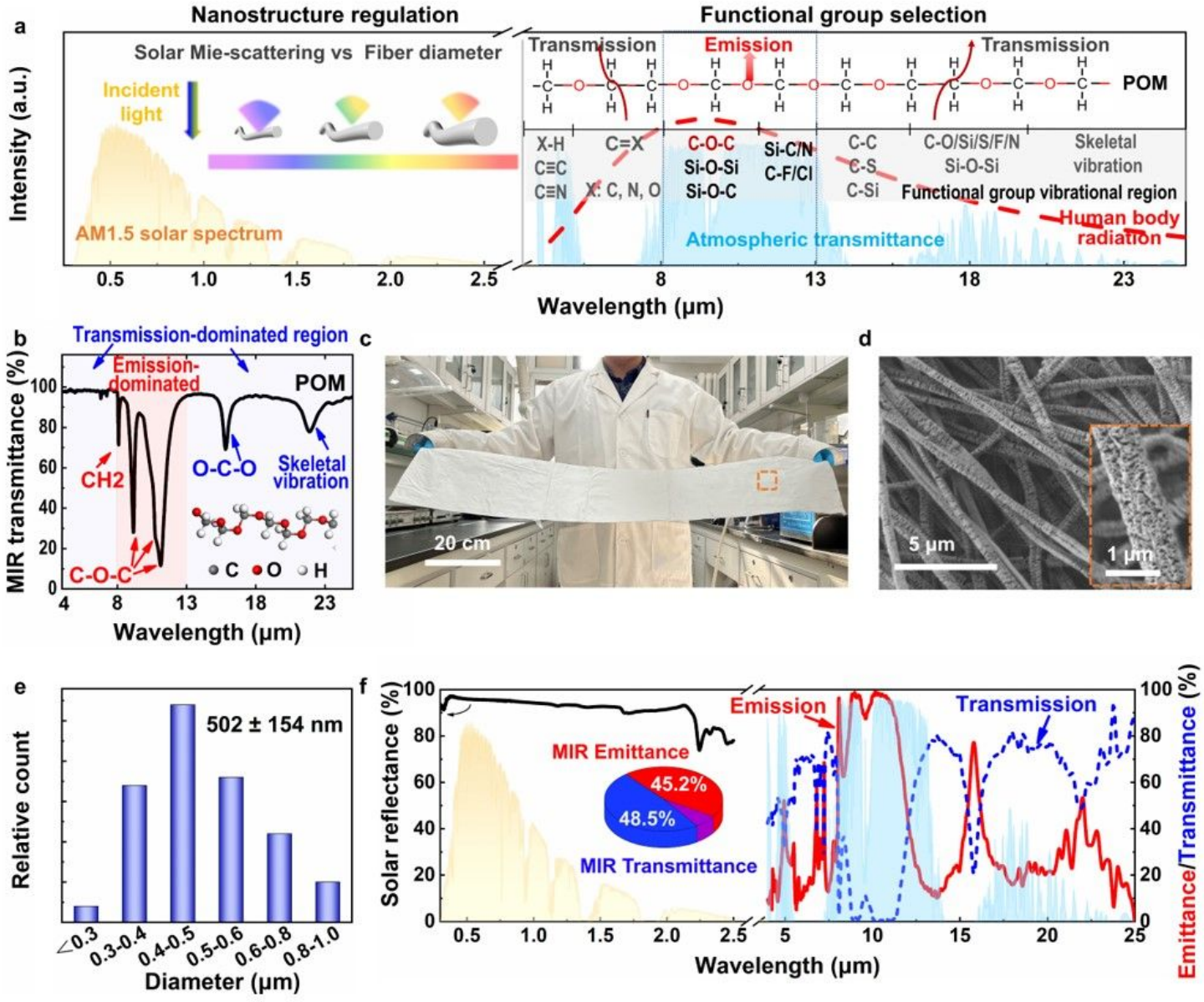

Figure 2

Design, preparation, and spectral analysis of the SET-type POM textile. a, Nanostructure regulation of SET-type textiles in the region of solar irradiation (left) and the functional group selection of POM in the MIR region (right). **b,** ATR-FTIR spectrum of POM where the main characteristic peaks of C-O-C vibrational absorption/emission are located in the region of the atmospheric window, and the other region is dominated by transmission. Inset is the schematic of the POM molecular chain. **c,** Photograph of the synthesized SET-type POM textile. **d,** SEM images of the POM nanofibers and the rough fiber surface (Inset). **e,** Statistical distribution of the diameters of the POM nanofibers. **f,** Spectral response of a 260 μm thick POM textile in the 0.3-25 μm wavelength range, including the solar reflectance (black line), MIR emittance (red line), and MIR transmittance (blue line). The inset shows the ratio of emittance, transmittance, and reflectance in the MIR region.

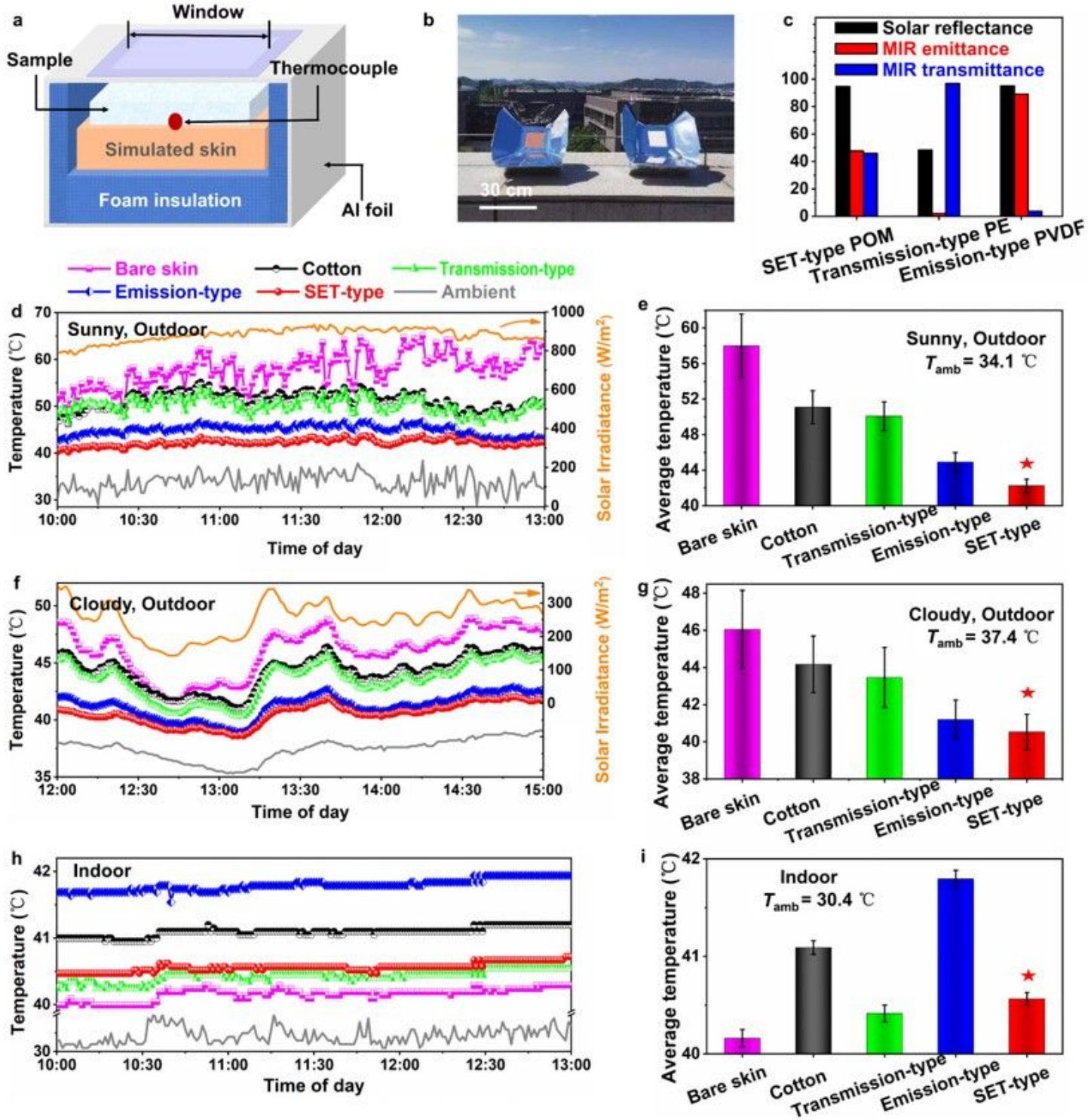

Figure 3

Multi-scenario human body cooling measurement of the SET-type POM textile, by comparison with bare skin and skin covered by commercial cotton, transmission-type PE, and emission-type PVDF. a, Schematic for the thermal measurement device used to characterize the radiative human body cooling performance in both outdoor and indoor scenarios. **b,** Photograph of the devices. **c,** Comparison of the solar reflectance, MIR emittance, and transmittance of SET-type POM, transmission-type PE, and emission-type

PVDF textiles. **d-i,** Thermal measurements in sunny outdoor (**d** and **e**, 03 May 2022), cloudy outdoor (**f** and **g**, 25 May 2022), and indoor (**h** and **i**, 19 May 2022) environments. The measurements include the real-time temperature (**d**, **f**, and **h**) and the corresponding average temperature (**e**, **g**, and **i**) of skin simulators wearing the different textile samples. Error bars in **e**, **g** and **i** indicate measurement variations of the samples at different time.

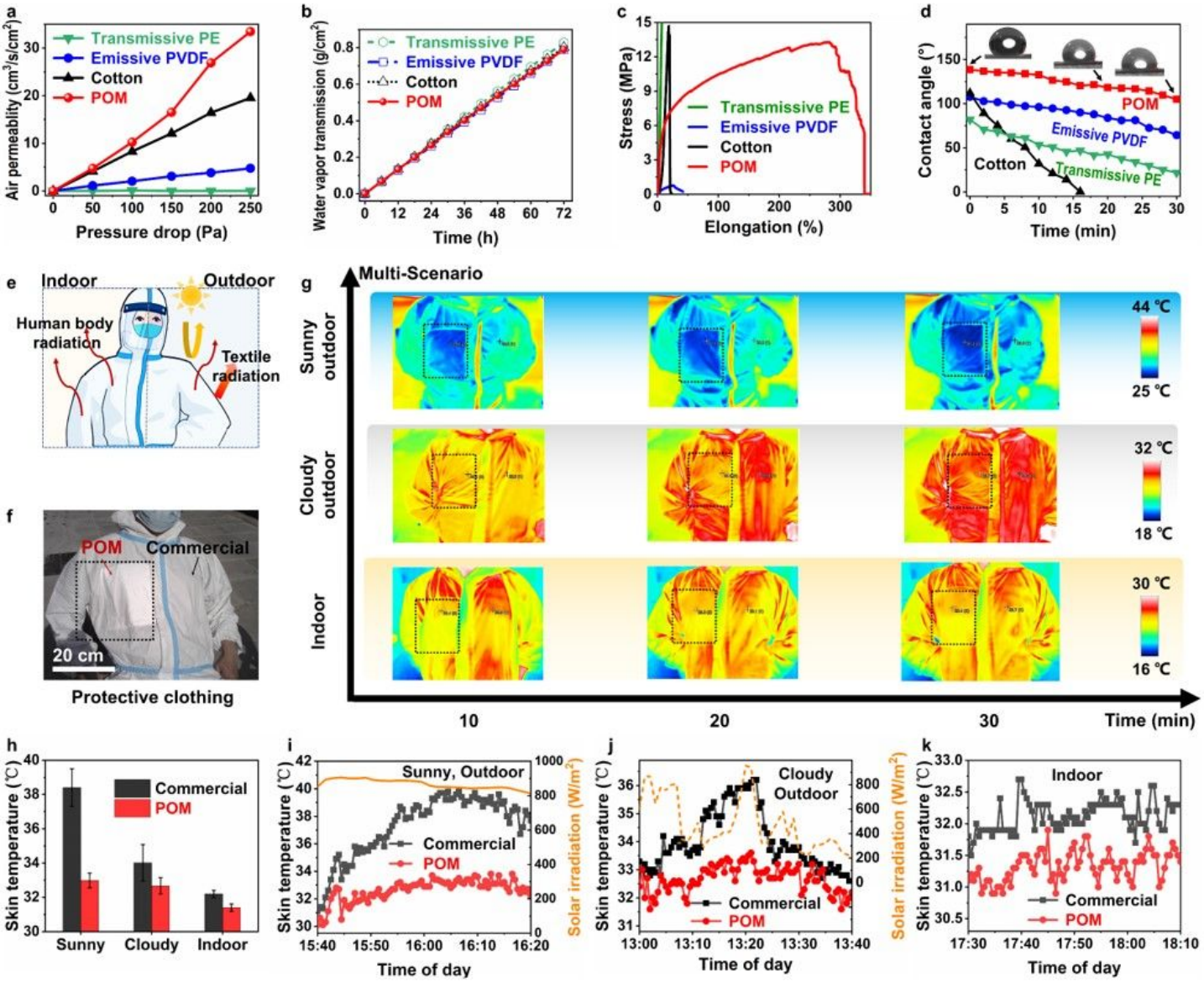

Figure 4

Wearability testing of the SET-type POM textile. a-d, Comparison of the wearability of SET-type POM, commercial cotton, emission-type PVDF, and transmission-type PE textiles (denoted as POM, Cotton, Emissive PVDF, and Transmissive PE, respectively), including an air permeability test (**a**), water vapor transmission rates versus time (**b**), mechanical strength test (**c**), and the water contact angle measured versus time (**d**). **e** and **f,** Schematic (**e**) and photograph (**f**) of a researcher wearing the POM textile based protective clothing. **g,** Infrared images of the researcher wearing the protective clothing in sunny outdoor

(16 May 2022), cloudy outdoor (17 May 2022), and indoor (17 May 2022) environments in Beijing, China (40°0'33" N, 116°20'0.6" E). **h,** The average temperature of skin under the two clothes in different scenarios. **i-k,** Real-time skin temperature in sunny outdoor (**i**, 24 May 2022), cloudy outdoor (**j**, 31 May 2022), and indoor (**k**, 25 May 2022) environments in Beijing, China. Error bars in **h** indicate measurement variations of the samples at different time.

Supplementary Files

This is a list of supplementary files associated with this preprint. Click to download.

- 2SupplementaryMaterials.docx
- MovieS1S5.zip